



OPEN

Nonlinear functional muscle network based on information theory tracks sensorimotor integration post stroke

Rory O’Keeffe¹, Seyed Yahya Shirazi^{1,6}, Seda Bilaloglu^{2,6}, Shayan Jahed¹, Ramin Bighamian³, Preeti Raghavan^{4,7}✉ & S. Farokh Atashzar^{1,5,7}✉

Sensory information is critical for motor coordination. However, understanding sensorimotor integration is complicated, especially in individuals with impairment due to injury to the central nervous system. This research presents a novel functional biomarker, based on a nonlinear network graph of muscle connectivity, called InfoMuNet, to quantify the role of sensory information on motor performance. Thirty-two individuals with post-stroke hemiparesis performed a grasp-and-lift task, while their muscle activity from 8 muscles in each arm was measured using surface electromyography. Subjects performed the task with their affected hand before and after sensory exposure to the task performed with the less-affected hand. For the first time, this work shows that InfoMuNet robustly quantifies changes in functional muscle connectivity in the affected hand after exposure to sensory information from the less-affected side. > 90% of the subjects conformed with the improvement resulting from this sensory exposure. InfoMuNet also shows high sensitivity to tactile, kinesthetic, and visual input alterations at the subject level, highlighting its potential use in precision rehabilitation interventions.

Stroke is a leading cause of long-term disability worldwide. As many as 76% of individuals with stroke experience upper-limb motor impairment at stroke onset¹. This impairment results from disrupted afferent and efferent neural transmission to and from the central nervous system (CNS), ultimately causing delayed initiation and termination of muscle contraction², slowness in developing forces, and disrupted processing and responsiveness to sensory feedback³. The collective firing of alpha motor neurons in the spinal cord activates motor units in the muscles, and their recruitment can be examined using surface electromyography (sEMG) to evaluate alterations in motor control^{4,5}. However, there are a variety of muscle activation parameters that can be altered as a result of stroke, which makes it difficult to find a parsimonious and consistently robust method to objectively evaluate changes in muscle coordination and motor control across individuals with stroke.

Stroke-induced motor impairments are more apparent in the contralesional limbs (affected side) than in the ipsilesional limbs (i.e., less-affected side)⁶. In addition, the location of the stroke lesion in the brain can have specific effects on motor and sensory processes^{7,8}. For example, a stroke in the right frontal region may impair temporal motor control on both the affected and less-affected sides, whereas a left parietal stroke may affect the spatial accuracy of upper limb reaching tasks^{8,9}. Specific stroke locations can produce selective visual, tactile, or proprioceptive sensory deficits, which also affect motor planning and performance^{10,11}. However, the less-affected side may provide critical sensory inputs to improve motor planning and performance on the affected side during functional tasks¹².

Rehabilitation after stroke is personalized based on the type and severity of the deficits and rehabilitation goals of the individual¹³. Quantifying the extent and severity of the impairments using standardized tools such

¹Department of Electrical and Computer Engineering, New York University, New York, NY, USA. ²Department of Medicine, New York University Langone Health, New York, NY, USA. ³Office of Science and Engineering Laboratories, Center for Devices and Radiological Health, United States Food and Drug Administration, Silver Spring, MD, USA. ⁴Departments of Physical Medicine and Rehabilitation and Neurology, Johns Hopkins University School of Medicine, Baltimore, MD, USA. ⁵Department of Mechanical and Aerospace Engineering, New York University, New York, NY, USA. ⁶These authors contributed equally: Seyed Yahya Shirazi and Seda Bilaloglu. ⁷These authors jointly supervised this work: Preeti Raghavan and S. Farokh Atashzar. ✉email: praghav3@jhmi.edu; f.atashzar@nyu.edu

as the Chedoke-McMaster Stroke Assessment and the Fugl-Meyer Scale can classify patients based on the level of impairment and track improvement with rehabilitation^{14,15}. However, these tools do not quantify sensorimotor integration and are not sensitive to subtle changes in functional motor coordination and control that may occur within a single session. Thus, there is an unmet need for objective functional biomarkers to track subtle changes in motor control, for example, in response to sensory feedback.

The spectrotemporal features of sEMG can, in theory, be the basis for a biomarker to monitor changes in motor control after stroke. This is because stroke alters the fluency of communication between the CNS and muscles, resulting in changes in sEMG activation patterns for everyday tasks¹⁶. Quantifying changes in sEMG using classical metrics such as the root mean square (RMS) amplitude^{16,17} and power spectral density (PSD)^{5,18,19} of muscle activity can be used to determine the intensity of muscle activation and the use of compensatory strategies. However, these metrics do not offer a means to combine the information from multiple muscles in a task-specific manner to assess coordination.

More advanced methods of sEMG processing such as low-frequency muscle synergies have been proposed to model coherence across muscle groups which play an imperative role in functional task performance^{20–22}. However, conventional muscle synergy analysis of the affected and less-affected limbs has shown similar patterns despite clear differences in motor performance. This suggests that muscle synergies may reflect spinal neural control²³ and may not provide the differential power needed to evaluate the shades of functional impairment caused by alterations in supraspinal neural control.

A more recent method for assessing functional connectivity across muscles computes the intermuscular coherence network which is a measure of the degree of information sharing across muscles necessary for sensorimotor control of movement^{24,25}. In this regard, a recent study on postural balance tasks showed that humans reorganize coherence-based muscle networks across limbs in the beta-to-gamma bands (20–60 Hz)²⁶. Coherence analysis across various muscle groups may represent the common input from the upper motor neurons to alpha motor neurons²⁷. This concept has been tested using invasive needle electromyography as a potential biomarker of upper motor neuron involvement in motor neuron disease²⁸. The connectivity between muscles at multiple distinct frequency bands demonstrates how muscle networks can be used to investigate the neural circuitry of motor coordination and provides insight about subtle motor control strategies that cannot be differentiated with other metrics, including muscle synergies²⁹.

While the recently-accelerated research on muscle connectivity has focused on the use of linear measures of same-frequency coherence (such as delta-band source to delta-band target)^{26,29,30}, cross-frequency connectivity and nonlinear coupling have not been investigated even though they can provide holistic insight into the distributed neural drive at the peripheral nervous system level. In this paper, we utilize the concept of mutual information rooted in Shannon's information theory to implement a nonlinear muscle network for stroke subjects. Mutual information has been proposed as an appropriate metric in connectivity analysis at the CNS level, for example in studying EEG-based functional brain connectivity. An example of a method that was proposed in the literature based on mutual information for connectivity analysis in the CNS is Weighted Symbolic Mutual Information (wSMI)^{31,32}. Information-theoretic measures of brain connectivity have shown the ability to detect neurological differences that were not detectable with linear measures^{33,34}, including the differentiation of patients with neurological disorders from healthy controls^{33,35,36}. To the best of the authors' knowledge, in the context of neurological disorders and injury (such as stroke), the use of such nonlinear metrics at the peripheral nervous system level has not been explored in the literature. In this paper, for the first time, we propose the concept of a nonlinear muscle network for stroke subjects and we explore the strength of such a nonlinear measure to characterize sensorimotor integration in these subjects.

Thus this paper focuses on the use of the functional muscle network as a potential biomarker for sensorimotor integration after stroke. We investigate a novel method for assessing temporal connectivity across 16 upper limb muscles (8 in each arm) using a network of nonlinear information-theory-based intermuscular coupling, called InfoMuNet, derived from processing the full-spectrum of sEMG recordings (Fig. 1).

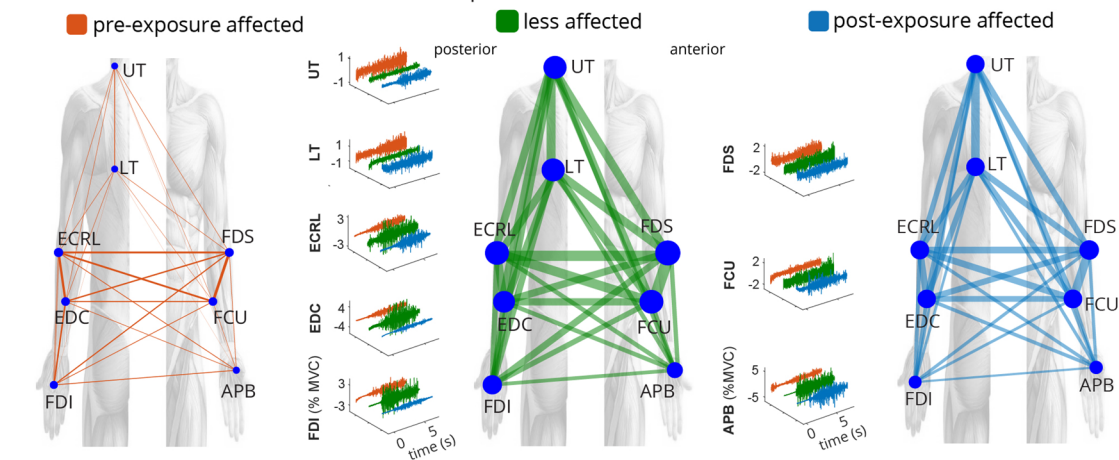
Thirty-two individuals with chronic post-stroke hemiparesis (21 males and 11 females, age: 57.9 ± 12.7 years, mean time since stroke: 46.4 ± 57.5 months, 15 with right hemiparesis and 17 with left hemiparesis) participated in a multiple-session grasp-and-lift experiment (Fig. 1c) during which their sEMG was recorded from 16 muscles, 8 on each limb. In a previous work, we showed that fingertip force coordination in the affected hand changes after exposure to the same task using the less-affected hand¹². Here, using sEMG, we quantify how sensorimotor exposure to the less-affected limb changes functional muscle coordination in the affected limb. The protocol utilizes alternating hand training (AHT), where the subject first performs the task with the less-affected hand to get exposed to sensory information and then performs the task with the affected hand (Fig. 1d).

The usefulness of the InfoMuNet approach is compared with that of the classical spectral and temporal metrics obtained using sEMG. The spectral and temporal features of the muscle activity signal (including RMS and PSD of the 16 sEMG channels) are compared with the degree, weighted clustering coefficient (WCC), mean shortest path, and global efficiency of InfoMuNet across the affected and less-affected limbs and various sensory conditions.

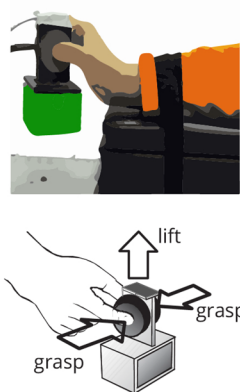
We hypothesized that (1) the connectivity metrics derived from InfoMuNet would sensitively capture changes in distributed muscle coordination in the affected limb after contralateral sensory exposure, whereas classical measures (i.e., RMS and PSD of sEMG) would not provide the needed separation power. In other words, although the absolute change in muscle activation may follow a heterogeneous pattern, the information sharing between muscles (that highlights coordinated projections of the CNS) shows an improved pattern after contralateral sensory exposure.

Moreover, we hypothesized that (2) InfoMuNet would show a discriminative sensitivity to contralateral sensory exposure to tactile, kinesthetic, and visual sensory inputs during task performance.

a. InfoMuNet and effect of sensorimotor exposure



b. grasp and lift task



c. task order



d. sensory conditions



e. mutual information

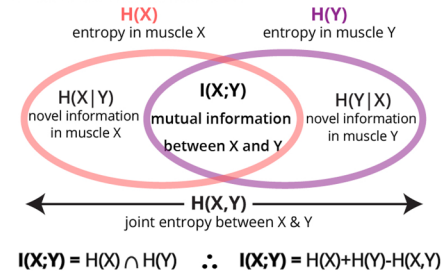


Figure 1. Grasp-and-lift task and InfoMuNet overview. **(a)** Electromyographic signals were recorded from eight muscles on each limb: Abductor Pollicis Brevis (APB), First Dorsal Interosseous (FDI), Flexor Digitorum Superficialis (FDS), Extensor Digitorum Communis (EDC), Flexor Carpi Ulnaris (FCU), Extensor Carpi Radialis Longus (ECRL), Upper Trapezius (UT), and Lower Trapezius (LT). The median InfoMuNet (i.e., the connectivity network of median mutual information between muscle pairs) across all subjects and trials indicates that the less-affected limb has the strongest connectivity during the grasp-and-lift task. The post-exposure affected shows stronger connectivity trends than the pre-exposure affected limb, highlighting the potential effect of sensorimotor exposure. sEMG plots are representative activations for each muscle. **(b)** For each trial, the task consisted of grasping the instrument with the thumb and index finger and lifting the instrument. **(c)** The experiment was completed in two separate sessions. Subjects performed the task with the affected limb only (pre-exposure affected) in the first session. Subjects performed the task first with the less-affected limb followed by the affected limb (post-exposure affected) in the second session. **(d)** The task was performed under eight sensory conditions. Subjects completed 14 trials for each sensory condition for a total of 112 trials (14 trials \times 8 sensory conditions = 112 trials). **(e)** Mutual information $I(X; Y)$ between signals from any two muscles is computed using the individual entropies $H(X)$, $H(Y)$, and joint entropy $H(X, Y)$. $I(X; Y)$ was quantified between all muscle pairs to form the InfoMuNet for each trial.

Results

This study evaluates changes in sensorimotor integration during a functional grasp-and-lift task before and after exposure to the less-affected limb post-stroke. Thirty-two subjects with chronic post-stroke hemiparesis performed a grasp-and-lift task (Fig. 1c) under eight different sensory conditions where visual, kinesthetic, and tactile inputs were varied in a random manner (Fig. 1e) over two sessions. At the first session, the task was performed with the affected hand only while sEMG was recorded from eight muscles in the affected limb (pre-exposure limb). In the second session, subjects performed the task first with the less-affected hand (exposure to preserved sensory information) immediately followed by the affected hand (post-exposure limb).

Subjects performed 112 trials each with the pre-exposure affected limb, post-exposure affected limb, and less-affected limb (14 trials \times 8 sensory conditions = 112 trials). For each sensory condition, two sets of 7 trials were performed, using a light and a heavy weight. The choice of the light and heavy weights was randomized between 8 different weight combinations ranging from 250 to 425 (light) and 500–675 g (heavy) in 25 g increments. We

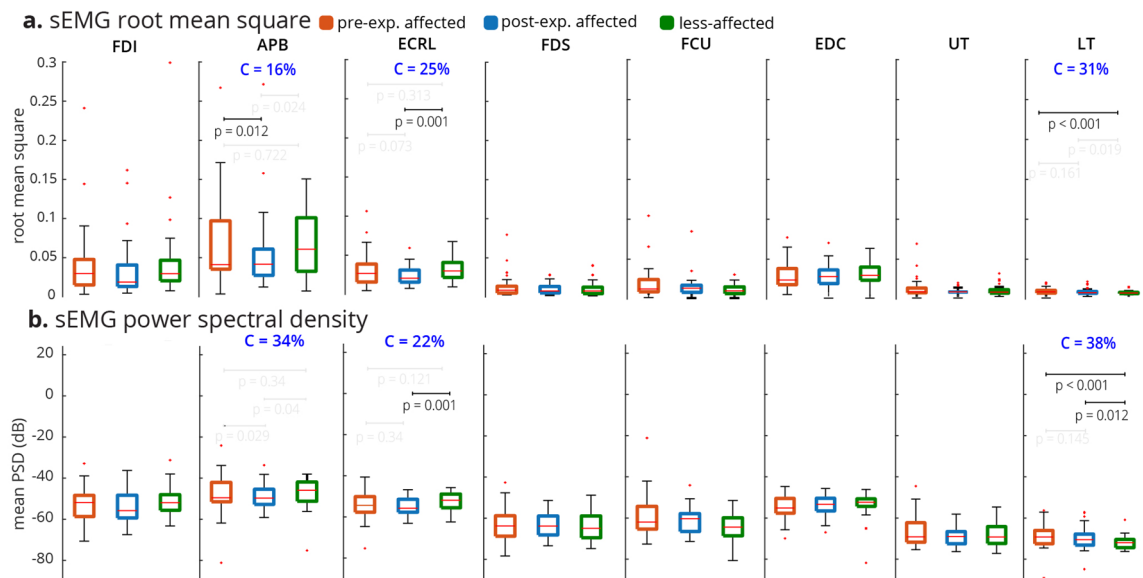


Figure 2. RMS and PSD of sEMG across $n = 32$ subjects. **(a)** For each electrode, the median RMS of sEMG envelope is quantified across all trials, and conditions per subject. Differences in the RMS values were only significant for the APB, ECRL, and LT muscles based on the Friedman test. The conformity ratio (the percentage of the subjects that followed the median group trend) for the significant comparisons was $C < 31\%$. **(b)** For each electrode, the median of mean-PSD is quantified across all trials and conditions per subject. The differences in PSD were significant for the APB, ECRL, and LT muscles based on the Friedman test. The conformity ratio for the significant comparisons was $C < 34\%$.

used the data from all the weight pairs for all subjects as one group because the preliminary analysis of the sEMG data did not indicate significant differences between light and heavy weights for the metrics used in this study.

Eight bipolar sEMG sensors (Delsys Inc, Natick, MA) were placed on the following muscles on each of the affected and less-affected limbs (Fig. 1a) over the muscle belly of the following muscles: Abductor Pollicis Brevis (APB), First Dorsal Interosseous (FDI), Flexor Digitorum Superficialis (FDS), Extensor Digitorum Communis (EDC), Flexor Carpi Ulnaris (FCU), Extensor Carpi Radialis Longus (ECRL), Upper Trapezius (UT), and Lower Trapezius (LT). Comparisons were made in the muscle activity of the pre-exposure affected, post-exposure affected, and less-affected limbs, considering the full task duration.

It should also be highlighted that for a clinically transferable robust sEMG-based biomarker, a linearly-trended behavior would be needed that monotonically changes going from pre-exposure affected, to post-exposure affected, to less-affected limbs in a consistent direction. This monotonicity is critical if it is claimed that a biomarker can detect subtle changes in the recovery process.

Classical spectrotemporal sEMG analysis. The classical spectral and temporal analyses of muscle activity using rectified sEMG and PSD showed heterogeneous trends across the muscles involved in the task (Figs. 2, 3). No consistent pattern was observed when comparing muscle activity in the pre-exposure affected, post-exposure affected, and less-affected limbs across the subjects and muscles, as explained below.

Only the APB, ECRL, and LT muscles demonstrated significant differences across the pre-exposure affected, post-exposure affected, and less-affected limbs using PSD and RMS metrics (Fig. 2) (*Friedman* $Chi^2_{(2,62)}$'s > 6.8125 , p 's < 0.05). There was a decreasing trend in activation of the LT muscle on both RMS and PSD from pre-exposure affected to post-exposure affected, to less-affected limbs, whereas for the APB and ECRL muscles, the post-exposure affected limb trended to have the smallest RMS and PSD. Conformity scores (i.e., the ratio of the subjects that followed the median group trend to all subjects) indicated that $\sim 30\%$ of the subjects followed the median group trend for RMS and PSD even though statistically significant differences were noted. As we can see in Fig. 3, the ensembled medians of RMS and PSD do not provide any significant trend and the Friedman tests also fail to recognize group effects between the pre-exposure affected, less-affected and post-exposure affected limbs (RMS: *Friedman* $Chi^2_{(2,62)} = 4.75$, $p = 0.0930$, PSD: *Friedman* $Chi^2_{(2,62)} = 3.25$, $p = 0.1969$). Only 22% of the subjects conformed with the ensembled RMS and PSD trends. Thus, while the classical spectrotemporal analyses of sEMG reveal potential changes in specific muscle activities from pre-to-post exposure to sensory information from the less-affected limb, the trends are not consistent across all muscles, and may not provide information about coordination across muscles involved in the task.

Time-frequency analysis. The time-frequency analysis provided the spectral power changes of the sEMG signal across the duration of the task using short-time Fourier Transform (STFT) (Fig. 4). The spectral power of the sEMG was divided into three spectral windows, 20–35 Hz (β band), 35–60 Hz (low γ band), and 60–200 Hz (high γ band), while the duration of the trials was normalized to ten temporal windows (0–10%, 10–20%, ...). Overall, the spectral power had a decreasing trend from pre-exposure to post-exposure for the affected

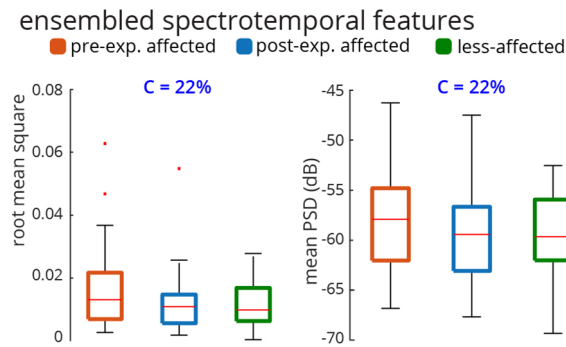


Figure 3. Ensembled RMS and PSD across $n = 32$ subjects. For each subject, the median RMS values across all sEMG electrodes, all conditions, and all trials are quantified. Thus, there is a distribution of 32 ensembled RMSs for 32 subjects. The same method is used for generating the distribution of ensembled PSD (considering 20 to 200 Hz). The Friedman test was not significant for either RMS or PSD of sEMG (RMS: *Friedman* $\chi^2_{(2,62)} = 4.75, p = 0.0930$, PSD: *Friedman* $\chi^2_{(2,62)} = 3.25, p = 0.1969$). The conformity ratio was equal for both RMS and PSD ($C = 22\%$).

time-frequency analysis

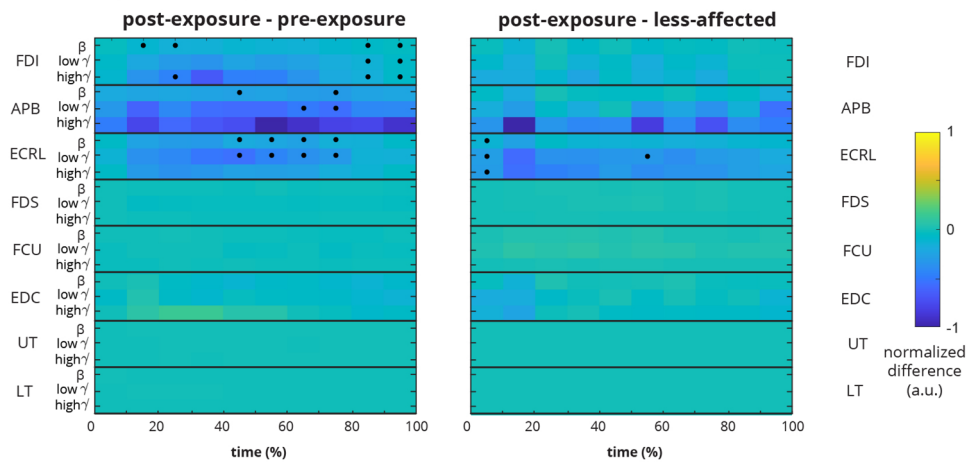


Figure 4. Time-frequency comparison of sEMG using STFT. **(Left)** The comparison of sEMG spectral power between pre-exposure and post-exposure affected limbs shows that FDI, APB, and ECRL muscles have overall decreases in spectral power during portions of the trials. **(Right)** The comparison of sEMG spectral power between post-exposure affected and less-affected limbs does not show significant spectral changes except for ECRL. The color of the boxes indicates the difference between the respective limbs normalized to the absolute maximum difference in each grid. Dots indicate a significant difference after accounting for multiple comparisons.

limb, as indicated in Fig. 4 by a blue hue. Only three muscles (FDI, APB and ECRL) demonstrated significant differences between the sessions for some part of the task duration (Fig. 4). ECRL showed significant spectral power decreases in β and low γ bands during the middle of the task. APB had also brief decreases in β and low γ at around 75% of the task duration. FDI's spectral power slightly increased near the end of the task for the post-exposure compared to the pre-exposure trials. The comparison between the post-exposure affected and the less-affected limbs did not yield statistical significance except for brief periods of ECRL activity.

InfoMuNet analysis. InfoMuNet was used to evaluate the nonlinear coupling of the eight muscles engaged in the functional task. Figures 1e and 5 show the median connectivity of the functional muscle network across the subjects, where for each subject the network was generated by computing the mutual information exchanged between each muscle pair. As expected, the results from the merged population indicate that the median mutual information degree in the functional muscle network increases monotonically from pre-exposure affected, to post-exposure affected, to the less-affected limbs, highlighting the functional importance and ease of interpretability of this method (Fig. 5a). The mutual information heatmap shows that the post-exposure affected limb demonstrated stronger pairwise coupling than the pre-exposure affected limb, especially for the FCU-FDS, EDC-ECRL, and FDS-ECRL muscle pairs involved in grasping and lifting using wrist extension, and in the

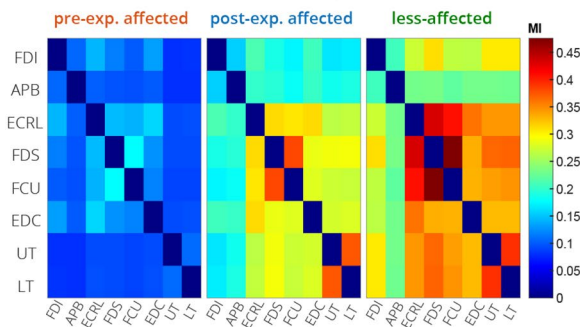
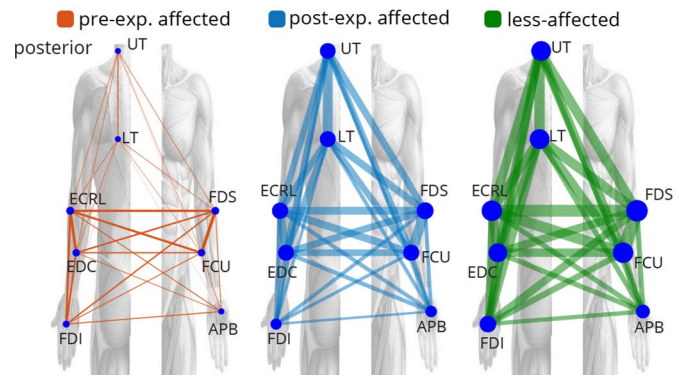
a. mutual information map**b. mutual information network**

Figure 5. The median InfoMuNet (i.e., the connectivity network of median mutual information between muscle pairs) across all trials of all subjects is shown in two different formats. **(a)** The mutual information heatmaps across all subjects show that the pairwise mutual information increases across all nodes (muscles) from the pre-exposure affected to post-exposure affected and less-affected limbs. **(b)** The mutual information networks also show an increase in both pairwise mutual information (the edges' line widths) and the muscles' degrees (the nodes' radii). MI = Mutual Information.

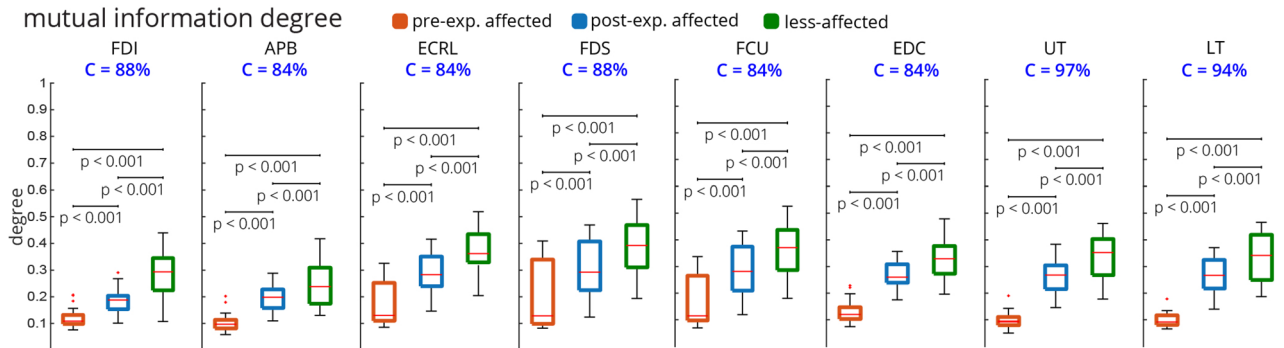
mutual information degree

Figure 6. Mutual information degree for individual muscles across all $n = 32$ subjects. For each subject, the mutual information degree was quantified for the median muscle network across all trials. All muscles showed a significant monotonic increase in degree from pre-exposure affected to post-exposure affected and less-affected limbs. The conformity for all muscles was $> 80\%$. The UT and LT muscles had the highest conformity at $\geq 94\%$.

UT-LT muscle pair involved in stabilizing the shoulder girdle (Fig. 5a). Importantly, the less-affected limb shows even stronger pairwise mutual information coupling than the post-exposure affected limb in these muscle pairs. Overall, the mutual information network became stronger pre-to-post exposure to the sensory information from the less-affected limb (Figs. 1e and 5).

As can be seen in Fig. 6, the mutual information degree (defined in the “Methods” section, a measure of mean connectivity of each muscle) of each muscle showed significant increases from the pre-exposure affected to post-exposure affected, to less-affected limbs ($Friedman\ Chi^2 > 50.8125, p < 0.001, post-hoc\ p's < 0.001$). Overall, high conformity was observed, and interestingly $\geq 94\%$ of the subjects conformed with this trend for the trapezius muscles (UT and LT).

Furthermore, additional network metrics also showed similar consistent trends from pre-exposure affected to post-exposure affected to less-affected limbs (Fig. 7). The mean mutual information degree (averaged across all muscles), overall showed 94% conformity. The mean WCC (defined in the “Methods” section, a measure of the extent to which the nodes, i.e. muscles, tend to group together), also increased significantly and consistently from pre-exposure affected, to post-exposure affected, to less-affected limbs and showed perfect conformity of 100%. The mean shortest path (defined in the “Methods” section, a measure of network sparsity), decreased from the pre-exposure affected to post-exposure affected to less-affected limbs, with 94% conformity. In addition, the global efficiency (defined in the “Methods” section, a measure of overall network connectivity), increased from pre-exposure affected to post-exposure affected to less-affected limbs also with perfect conformity of 100%.

We also investigated the effect of sensory manipulation on the topological changes in the InfoMuNet. Availability of tactile, kinesthetic, and visual sensory inputs changed the mean degree, conformity, and difference between the post-exposure affected and less-affected limbs (Fig. 8). The mean mutual information degree increased from the pre-exposure affected, to post-exposure affected, to less-affected limbs for all sensory conditions ($Friedman\ Chi^2 > 41.8125, p < 0.001, post-hoc\ p's < 0.002$), as seen in Fig. 8a. The conformity was the highest at 97% with the lack of any sensory feedback (all blocked, Fig. 8a), suggesting that subjects had the most consistent behavior under this condition. The conformity consistently decreased as more sensory information

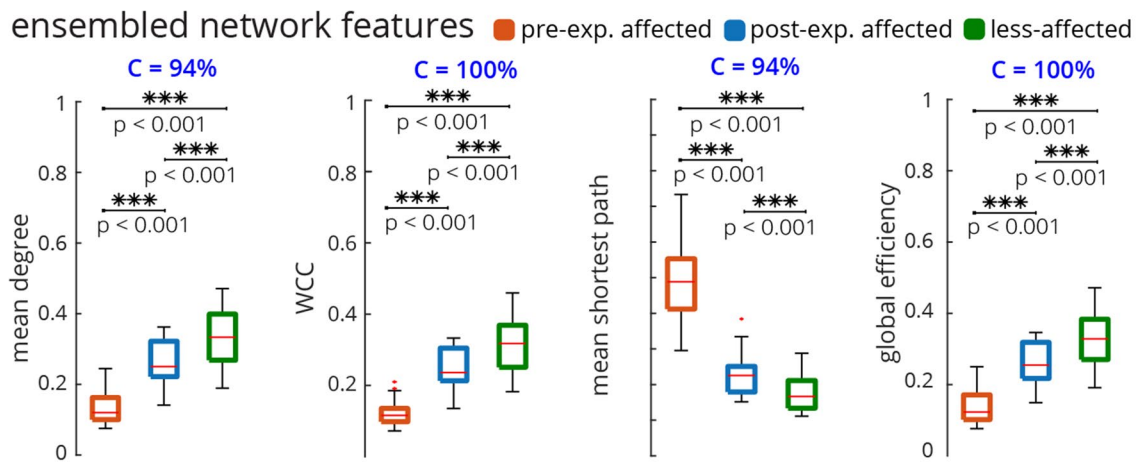


Figure 7. The ensembled metrics of the mutual information network across all $n = 32$ subjects. For each subject, the median muscle network across all trials was computed. Then, the four metrics shown were computed for this ensembled network. All network metrics monotonically changed from pre-exposure affected to post-exposure affected and less-affected limbs. The mean WCC and global efficiency had perfect conformity, $C = 100\%$. WCC: weighted clustering coefficient.

was added and was the least at 75% when all tactile, kinesthetic, and visual sensory inputs were provided; this decreasing trend in conformity suggests that inter-individual differences exist in the availability and processing of multiple sensory inputs carried from the less-affected limb, which in turn, influences the functional muscle network connectivity in the affected limb after exposure. The importance of sensory information for muscle coordination was quantified by the ratio of the mutual information degree of the post-exposure affected limb to that of the less-affected limb. A mean ratio of 1 implies that the post-exposure affected limb has similar network behavior to the less-affected limb. In the presence of tactile, kinesthetic, and visual sensory feedback, the ratio was significantly higher (i.e., closer to one) than in the absence of sensory feedback (Fig. 8b) (*Wilcoxon sign-rank test*, $p = 0.004$). This result highlights the importance of the transfer of sensory input from the less-affected to the affected hand and its role in improving functional muscle network connectivity, which was robustly captured by the InfoMuNet approach.

Discussion

The results show that the information theory-based muscle network (InfoMuNet) can encode nonlinear functional muscle coordination as a robust biomarker of sensorimotor integration after stroke with $> 90\%$ conformity of the individuals to the group trends. For the first time, we show that the contralateral sensory exposure in chronic stroke patients can result in significant improvement of muscle coordination, quantified by InfoMuNet. This demonstrates the importance and potential for sensory-based rehabilitation and the possibility of improving muscle coordination in the chronic post-stroke population. The functional muscle network also exhibits high sensitivity to the contribution of specific tactile, kinesthetic, and visual sensory inputs for motor coordination. Our results highlight the role of sensory inputs from the less-affected limb to improve functional muscle coordination in the affected limb post-stroke, using the AHT protocol. On the other hand, the spectrotemporal characteristics of sEMG signals fail to capture such changes in muscle activity in a consistent manner. The results highlight the importance of the proposed functional muscle network for tracking progress towards recovery during rehabilitation.

The analysis of sEMG activity showed that muscles have a wide range of temporal and spectral variability during the grasp-and-lift task. Conventional temporal (RMS) and spectral (PSD) characterizations of sEMG activations show that specific muscles, specifically the APB and ECRL muscles demonstrate significant changes in activation from pre-to-post exposure in the affected limb, consistent with their importance in sensing object weight during the grasp-and-lift task as shown previously^{37,38}. However, the conformity of subjects to the ensembled median group trend was only 22%. The seemingly wider RMS boxplots for FDI, APB, ECRL, and EDC are likely related to the utility of these muscles during the task, different strategies subjects used to recruit these muscles, or potential compensatory mechanisms to successfully complete the tasks. The ensembled group trend was not statistically significant, indicating that subjects demonstrated heterogeneous spectrotemporal trends (Fig. 3) before and after exposure of the less-affected limb to the grasp-and-lift tasks. The time-frequency STFT analysis also demonstrated a similar pattern indicating that only the spectral power of FDI, APB and ECRL changed from pre-exposure to post-exposure in the affected limb, mainly in β and low γ bands (Fig. 4). The conventional metrics also produced inconsistent relationships across muscles (as seen in Fig. 2), suggesting that spectrotemporal features are not well-suited to use as a biomarker for coordination across muscle groups.

However, as hypothesized, we show for the first time that the InfoMuNet method provides a consistent, uniform gradient (Figs. 5, 6, 7, 8) which highlights its potential as a robust functional biomarker of coordination across muscle groups. The monotonicity of InfoMuNet was validated by computing the mutual information degree of network connectivity, and the results showed a consistent improvement in functional muscle network

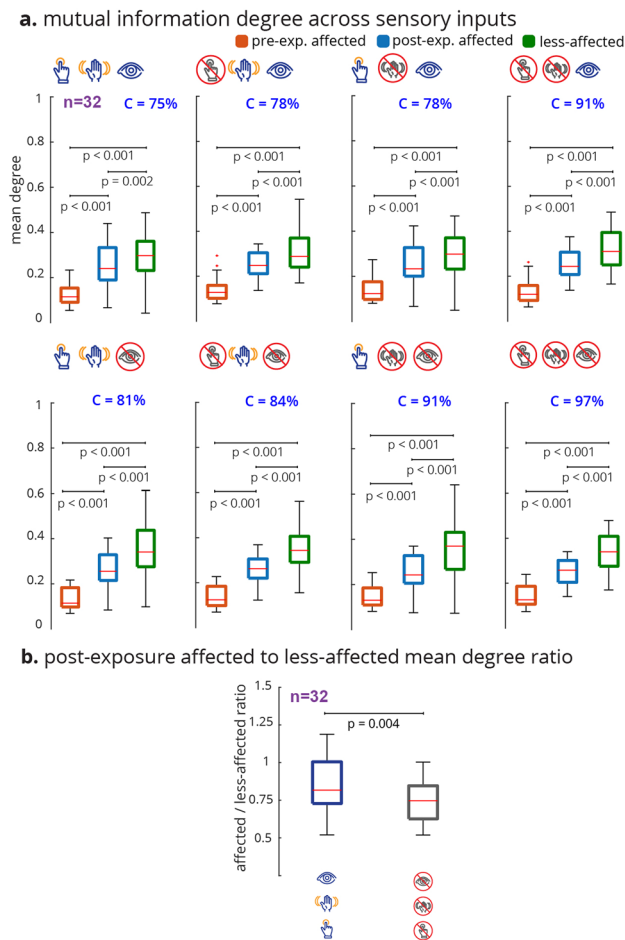


Figure 8. The mutual information degree across sensory conditions. For each subject and sensory condition, the median muscle network across all trials was computed. The mean degree was then calculated for that median muscle network. **(a)** For all conditions, the mean degree ascended monotonically with statistical significance from pre-exposure affected to post-exposure affected to less-affected limbs. **(b)** The ratio of the post-exposure affected to less-affected mean degree distributions was computed for all (none blocked) vs no (all blocked) sensory feedback conditions. Wilcoxon sign rank test shows a significant difference between the mean degree ratio distributions. The affected limb's muscle network approached that of the less-affected limb with sensory feedback compared to without sensory feedback.

connectivity from pre-to-post exposure in the affected limb and high discriminative power in distinguishing between the less-affected and post-exposure affected muscle networks. The objective measures of connectivity (e.g., degree and WCC) revealed a consistent trend, where the less-affected limb always had a better score when compared to the post-exposure affected limb. Similarly, the post-exposure affected limb demonstrated a better score compared to the pre-exposure affected limb across all muscles (Fig. 6); and the trend was consistent for the overall network as well (Fig. 7). Thus, for the first time, this paper shows that the connectivity between the muscles calculated using mutual information (i) is highest for the less-affected limb compared to the affected limb, (ii) increases in the affected limb after exposure to the less-affected limb, and (iii) provides $\geq 94\%$ average conformity across the subjects (Fig. 7). To the best of the authors' knowledge, this is the first time that information theory has been used to generate a functional muscle network. This is also the first time that the functional muscle network has been used to track changes in sensorimotor integration after stroke.

Stroke tends to increase the variability in the firing rate of the alpha motor neurons³⁹, which may explain why nonlinear coupling between muscles is lower in the affected limb. The high conformity of the subjects to the group trends and the high gradient uniformity of the trajectory across the less-affected, post-exposure affected, and pre-exposure affected limbs suggests that InfoMuNet can be used as a biomarker to distinguish differences between the affected and less-affected limbs, and track progress during rehabilitation and recovery. This paper provides the first evidence that, in contrast to the weak and heterogeneous performance of conventional metrics, InfoMuNet is a robust method to track motor coordination during functional task performance as shown here in the context of a sensory exposure paradigm. Moreover, since subjects were not selected based on the location of the lesion, it can be concluded that InfoMuNet was successful in capturing the changes in muscle connectivity despite the inherent heterogeneity in the stroke population.

The subjects in this study were in the chronic stage post-stroke and were not receiving active rehabilitation at the time of the study. Furthermore, the testing sessions were performed within a few days of each other. Hence, the changes in functional muscle connectivity cannot be attributed to natural recovery. Thus, exposure to the less-affected limb is the likely cause of improved network performance in the affected limb. In a previous study, we showed that sensorimotor exposure to the less-affected limb can improve fingertip force coordination in the affected limb after stroke¹². However, this is the first time that changes in functional muscle network connectivity have been examined. Improved motor coordination in the affected limb after exposure to the less-affected limb may be due to the transfer of information at the spinal or supraspinal levels. Previous studies have shown that central pattern generators (CPGs) may be responsible for the transfer of learning across limbs^{40–42}. CPGs can have spinal or supraspinal origins, hence further research is needed to determine the mechanism underlying this improvement⁴³.

In this paper, we also investigated the differential effect of providing tactile, kinesthetic, and visual sensory inputs (Fig. 8). The results show that InfoMuNet is responsive to changes in sensory feedback and reflects how sensory information is used for muscle coordination during sensorimotor integration. It should be highlighted that as the sensory conditions changed, the difference in functional muscle network connectivity captured by InfoMuNet was statistically differentiable across the affected and less-affected limbs (Fig. 8). This further confirms the role that sensory inputs play in motor coordination, and InfoMuNet is robust enough to discriminate the effect of specific sensory inputs on task-specific functional motor coordination after stroke. Examining the ratio of the mean degree of connectivity between the affected and less-affected limbs between all-sensory vs no-sensory feedback showed that the muscle network of the affected limb significantly improves toward that of the less-affected limb with the addition of sensory feedback (Fig. 8b). While the motor task could still be performed in the no sensory feedback condition, sensory feedback augmented sensorimotor control and task-specific intermuscular coordination, further reinforcing the use of InfoMuNet as a biomarker of sensorimotor integration.

Muscle synergy analysis is another approach to quantifying the activation patterns across muscles, in which an estimated low-dimensional vector of muscle weights (W) and a corresponding vector of time-varying activation coefficients (A) build the overall muscle activity⁴⁴. The complexity of W can differentiate the motor skills and different control strategies, while A is indicative of how much each element of W is recruited for a given task. Synergy analysis has been successful in differentiating skilled versus non-skilled actions, various postural balance conditions, healthy subjects, and stroke patients^{45–47}. However, previous studies did not indicate changes in W caused by stroke in the patient group (for example one W for the affected and another W for the less-affected limb). In contrast, previous studies supported the notion of having the same W 's for both affected and less-affected limbs in stroke patients and emphasized the changes only in the activation coefficients (A)^{23,48}. This suggests that synergy reflects mainly spinal control²³ and does not indicate supraspinal changes associated with stroke. Hence, muscle synergy analysis may not be a robust biomarker for tracking progress in stroke rehabilitation and recovery.

The strong statistics, high conformity, and high gradient uniformity of the results using InfoMuNet suggest that a mutual information-based connectivity approach can be used as an objective biomarker for monitoring recovery. Over 90% of the subjects conformed to the median group network trends, suggesting that the InfoMuNet metrics are strong indicators for functional motor coordination after stroke and can sensitively capture changes during the course of recovery (Fig. 7). It should be highlighted that the InfoMuNet metrics had substantially greater conformity than the RMS or PSD metrics and were robust to the inherent intersubject variability present in patients with stroke. Given that existing measures of motor function after stroke do not take sensory feedback into account^{14,15,49,50}, InfoMuNet offers quantification of sensorimotor integration, not just motor capability, which is critical for coordinated functional performance. Major advantages in using InfoMuNet for the analysis of muscle activity are the objectivity of the metric, the ability to test sensorimotor integration, and the potential to provide real-time feedback on task performance.

This study examined a heterogeneous group of subjects with chronic stroke at a cross-section in time, precluding an understanding of the effect of time and intervention on post-stroke recovery of sensorimotor integration. Furthermore, subjects presented at various times post-stroke. We also did not control for the side of the stroke. Previous studies have suggested that hemispheric specialization and lesion location can affect motor control⁸. However, despite this heterogeneity, InfoMuNet emerged as a robust functional biomarker which speaks to its broadest applicability. In future studies, we will be able to tease out the effect of stroke-specific characteristics on motor coordination.

In conclusion, InfoMuNet is proposed as a novel, robust functional biomarker of muscle network connectivity required for task performance. It can be used to assess progress in sensorimotor integration and functional performance in patients post-stroke. The results of this paper shed light on the importance of sensory-based motor training to promote healthier coordination of muscle activation. This is a significant observation for chronic post-stroke patients. In a grasp-and-lift task, InfoMuNet successfully differentiated intermuscular coordination in the affected limb after exposure to the less-affected limb. The objective nature of the network metrics and the > 90% conformity of individual subjects to the median group trend makes InfoMuNet a strong candidate for future closed-loop assessments of rehabilitation techniques, as it can evaluate both sensory and motor effects on task performance. Its responsiveness to sensory information makes it highly sensitive to even single-session rehabilitation interventions that may predict longer-term responsiveness to interventions, laying the foundation for precision rehabilitation. Future studies on functional muscle network characteristics in individual subjects and their responsiveness to short-term interventions, as well as their long-term effects, will help delineate the underlying neurophysiological processes that influence the recovery of functional muscle networks after stroke and other supraspinal neurodegenerative conditions.

Methods

Thirty-two patients with chronic stroke (11 females, 21 males, 57.91 ± 12.7 years, mean time since stroke: 46.4 ± 57.5 months, 15 with right hemiparesis and 17 with left hemiparesis) participated in the study. The study was approved by the Institutional Review Board of the New York University (IRB No: S12-03117) and was conducted in accordance with the Declaration of Helsinki. All participants provided their written consent prior to participation in the study. The inclusion criteria were: ability to read/write in English, age > 18 yrs, radiologically verified stroke > 4 months old, moderate arm motor impairment (Fugl-Meyer Scale < 60/66), ability to reach, grasp and lift the test objects with the affected side as assessed by the specialist, willingness to complete all clinical assessments and MRI, and comply with training protocols, ability to give informed consent and HIPPA certifications. The exclusion criteria were: sensorimotor impairments in the unaffected hand, severe visual or sensory impairment, including neglect on the affected side, significant cognitive dysfunction (score < 24 on Folstein's Mini Mental Status Examination), severe or unstable spasticity on treatment with Botulinum toxin or intrathecal baclofen, major disability (modified Rankin Scale > 4), and previous neurological illness, complicated medical condition, or significant injury to either upper extremity.

Grasp-and-lift task. Subjects completed a series of grasp-and-lift tasks while their muscular activity was recorded (Fig. 1b). The task was to grasp a custom-made instrumented device using the thumb and index fingers and lift it by extending the wrist. The task was performed under eight randomly assigned sensory conditions that allowed or blocked a combination of tactile, kinesthetic, and visual feedback during the task (Fig. 1d). Vision was blocked using a blindfold. Tactile feedback was altered by placing a layer of foam on the subject's grasping fingertips. Kinesthetic feedback was limited by blocking movement of the wrist using a splint. The arm was placed on an elevated platform and the subject held the object in the air by grasping the device between the thumb and the index finger.

Subjects performed the study over two separate testing sessions: one where they used the affected hand only and a subsequent session during which subjects performed Alternating Hand Training (AHT), where they first grasped and lifted the object with the less-affected hand followed by the affected hand (post-exposure) (Fig. 1c). Subjects performed 7 repeated trials in two sets, each with a light and heavy weight for all sensory conditions. Each trial consisted of a single repetition of the grasp-and-lift motion. The less-affected limb trial was immediately followed by the post-exposure affected trial. Subjects were given rest as required between trials. Using the non-parametric Friedman test, the sEMG data did not show significant differences for the spectrotemporal or network metrics. Therefore, we grouped all the weight pairs and performed the analysis on all trials. In total there were eight sensory conditions, and 14 ($7 \times 2 = 14$) trials per sensory condition amounting to 112 trials each with the affected limb pre-exposure, with the less-affected limb, and with the affected limb post-exposure to sensorimotor information from the less-affected limb per subject.

Data acquisition and spectrotemporal analysis. A wireless sEMG system (DE2.1 Sensors, Delsys Inc., Natick MA) was used to collect sEMG signals from 16 electrode locations, 8 in each limb (Fig. 1a). The recorded muscles were: Abductor Pollicis Brevis (APB), First Dorsal Interosseous (FDI), Flexor Digitorum Superficialis (FDS), Extensor Digitorum Communis (EDC), Flexor Carpi Ulnaris (FCU), Extensor Carpi Radialis Longus (ECRL), Upper Trapezius (UT), and Lower Trapezius (LT). The sEMG signals were pre-amplified and sampled at 2000 Hz, then normalized to the maximum voluntary contraction of each muscle for a given subject. The maximum voluntary contraction was determined by asking the subject to perform maximal isometric contraction of the given muscle for 3s. The maximum activity over the peak 1s was used for normalization.

Data were processed offline using custom functions in MATLAB R2020b (Mathworks Inc., Natick, MA). Signals were band-pass filtered between 20 and 200 Hz, with notch filters at multiples of 60 Hz. The PSD was calculated using the filtered signal by applying Welch's method with a Hamming window of length 0.85s and 50% overlap. For Figs. 2 and 3, the mean PSD of sEMG in 20–200 Hz was considered for each trial. The Hilbert transform was applied on the filtered and rectified signal to obtain the sEMG envelopes, which were used for RMS computation. For both the spectral (PSD) and temporal (RMS) feature computation, the full task duration was considered.

Time-frequency analysis. The time-frequency analysis provides the changes in the frequency context of the multiple sEMG channels over the conduction of the task. Here we utilized the STFT approach to generate the time-frequency analysis. The task's start time was defined as when the linear envelope increased beyond 10% of the maximum value and the end time was defined as when the falling linear envelope decreased to less than 10% of the maximum value. The STFT of each muscle was computed using a Hamming window, Fast-Fourier Transform (FFT) length of 0.212s, and 50% overlap. Afterward, the STFT results were reduced to ten data points representing normalized segments of the task (0–10%, 10–20%, ...). The mean spectral power in the 20–35 Hz (β band), 35–60 Hz (low γ band), and 60–200 Hz (high γ band) frequency ranges were quantified for each trial. The median across each subject's trials was computed for each limb. The differences (i) between post-exposure affected and pre-exposure affected limbs and (ii) between post-exposure affected and less-affected limbs were quantified for each muscle, frequency band, and time segment with the median across the 32 subjects. The difference values in the boxes were normalized by the maximum absolute difference in each grid of Fig. 4, hence each grid has a range between – 1 and 1. The color of each box is scaled in proportion to the difference.

The InfoMuNet approach. After band filtering between 20 and 200 Hz (with notch filters at multiples of 60 Hz), the sEMG signals were used to quantify the mutual information and construct the connectivity network

(InfoMuNet). Mutual information is a metric derived from information theory, which captures nonlinear couplings between two signals $x(t)$ and $y(t)$, by computing their individual and joint entropies.

Before computing the entropy, each signal is normalized over the full task duration and then discretized by using the Freedman-Diaconis⁵¹ method to choose the number of bins, N_b . The discretized version of $x(t)$ is denoted as X , and discretized $y(t)$ is Y . The probability distribution, $P_X(X_i)$, gives the distribution of the discretized signal X and was computed by constructing a histogram from all time samples per trial, with N_b equally spaced bins. The entropy of X , $H(X)$ —i.e. the uncertainty of $x(t)$ —is given as:

$$H(X) = - \sum_{i=1}^{N_b} P_X(X_i) \log_2 P_X(X_i). \tag{1}$$

The same method was used to construct the probability distribution for Y and hence compute $H(Y)$, the uncertainty associated with $y(t)$. The joint entropy, $H(X, Y)$, or joint uncertainty, is inversely proportional to the signals' inter-dependence and is the final term needed for finding the mutual information. For this, the joint probability distribution for X and Y , $P_{X,Y}(X_i, Y_j)$ should first be constructed by finding the empirical probability that X_i and Y_j are both in a given bin. Then, the joint entropy, $H(X, Y)$ is given as:

$$H(X, Y) = - \sum_{i=1}^{N_b} \sum_{j=1}^{N_b} P_{X,Y}(X_i, Y_j) \log_2 P_{X,Y}(X_i, Y_j). \tag{2}$$

Considering the entropy Venn diagram (Fig. 1d), the mutual information is computed as:

$$I(X; Y) = H(X) + H(Y) - H(X, Y). \tag{3}$$

Note that $I(X; Y)$ can alternatively be computed as:

$$I(X; Y) = H(X, Y) - H(X|Y) - H(Y|X). \tag{4}$$

where $H(X|Y)$ and $H(Y|X)$ represent the novel entropies of X and Y respectively.

Mutual information ($I(X; Y)$) can be defined as the amount by which a measurement of $y(t)$ reduces the uncertainty of estimating $x(t)$ ⁵². When $x(t)$ is completely independent of $y(t)$, the mutual information is zero. However, if $x(t)$ and $y(t)$ are identical time series, the mutual information is maximal. Unlike other connectivity measures such as Pearson correlation, the mutual information ($I(X; Y)$) between two signals is capable of capturing nonlinear and cross-frequency relations^{53–55}. For example, if $y(t)$ and $x(t)$ share a sinusoidal relation ($y(t) = \sin(x(t))$), the resultant $I(X; Y)$ is maximal while the computed Pearson correlation is approximately 0.

The median of mutual information for each muscle pair across trials was quantified, resulting in the median muscle network, which can be represented by adjacency matrix A . Using A , the following network connectivity metrics (nonlinear temporal features) were determined: (1) network degree, (2) weighted clustering coefficient (WCC), (3) shortest path, and (4) global efficiency.

1. The (mean) network degree gives an average connectivity for the network. The degree of a node (D_i) is the mean mutual information defining the edges connected to that specific node, as given below:

$$D_i = \left(\frac{1}{N-1} \right) \sum_{j=1, j \neq i}^N A_{ij}, \tag{5}$$

where N is the number of nodes. Then, mean network degree, $\bar{D} = \sum_{i=1}^N D_i$, is the mean of all nodes' degrees.

2. Mean WCC gives the measure of the extent to which nodes in a graph tend to group together. A node's weighted clustering coefficient (WCC_i) gives a relative measure of how well node i is connected to its neighbors (A_{ij}, A_{ik}) while also accounting for the neighbors' interconnection (A_{jk}). A node's clustering coefficient (CC_i) can be considered the sum of the triangles ($\sum_i t_i$) connected to node i , normalized by the maximum possible value⁵⁶.

$$CC_i = \frac{2 \sum_i t_i}{(N-1)(N-2)} \tag{6}$$

Each triangle's value will be the product of the three edges, $t_i = A_{ij}A_{ik}A_{jk}$. The weighted adjacency matrix \tilde{A} is scaled by the maximum connection in the network, hence $\tilde{A}_{ij} = A_{ij}/\max(A)$. The node's weighted clustering coefficient WCC_i is then defined as:

$$WCC_i = \frac{2}{(N-1)(N-2)} \sum_{j,k} (\tilde{A}_{ij}\tilde{A}_{ik}\tilde{A}_{jk})^{(1/3)} \tag{7}$$

A node which has (i) 0 connectivity to its neighbors or (ii) has neighbors whose interconnections are all 0 will have $WCC_i = 0$, while a node which is (i) maximally connected to its neighbors and (ii) has neighbors whose interconnections are all maximal has $WCC_i = 1$. Note that the value of WCC_i is more dependent on node i 's connections to its neighbors ($\tilde{A}_{ij}, \tilde{A}_{ik}$ terms) rather than the neighbors' interconnections (\tilde{A}_{jk} term). The mean WCC, $\overline{WCC} = \left(\frac{1}{N}\right) \sum_{i=1}^N WCC_i$, is the mean WCC over all nodes.

- The mean shortest path, also called characteristic path length, is inversely proportional to how well the network is connected overall. The shortest path between a node pair (muscle i , and muscle j) is defined as the minimum “connectivity path” (L_{ij}) between two nodes. A connectivity path between nodes k and l is $1/A_{kl}$. However, the shortest path is the minimum sum of paths to travel from k to l . The shortest path between all nodes in the network was computed using Dijkstra’s algorithm⁵⁷, and the mean shortest path \bar{L}_{ij} was calculated. The mean shortest path is bounded between 1 (a very well-connected network) and ∞ (a network with ubiquitously zero connectivity).
- Global efficiency is directly proportional to how well the network is connected overall. The efficiency (E) of a network is defined as:

$$E = \frac{1}{N(N-1)} \sum_{i \neq j} \frac{1}{L_{ij}}. \quad (8)$$

The efficiency (E) is normalized by the ideal efficiency (E_{id}) to give the global efficiency, GE :

$$GE = \frac{E}{E_{id}}, \quad (9)$$

which, unlike mean shortest path, is bounded between 0 and 1. A network with perfect connectivity will have $GE = 1$, while one with no connectivity will have $GE = 0$.

Statistical analysis. The Kolmogorov-Smirnov test for normality rejected the normal distribution hypothesis for the median PSD, RMS, and connectivity metrics across subjects (PSD: $p < 0.001$ for all of pre-exposure affected, post-exposure affected, and less-affected, RMS: $p < 0.001$ for all of pre-exposure affected, post-exposure affected and less-affected, connectivity metrics: $p < 0.001$ for all of pre-exposure affected, post-exposure affected and less-affected). Therefore, non-parametric statistical tests were used in our analysis. The Friedman test was used to compare spectrotemporal and connectivity measures between the pre-exposure affected, post-exposure affected, and less-affected limbs. The Wilcoxon signed-rank test was used for post-hoc tests if the Friedman revealed significance. Wilcoxon signed-rank test was used to determine the influence of sensory inputs on the network mean degree ratio. Wilcoxon signed-rank test was used to compare (i) pre vs. post-exposure affected limbs and (ii) post-exposure affected vs. less-affected limbs during the time-frequency analysis. The presence of a dot in Fig. 4 indicates a significant difference in the comparison for that particular muscle, frequency band, and time segment. Bonferroni correction was used to account for the multiple comparisons for the post-hoc tests. The significance level for all tests was set at 0.05.

Conformity was quantified as the ratio of the subjects that followed the median group trend. The percentage of the individual subjects that had the same trend as the median group trend was then measured.

To compare the effect of sensory information on the muscle network, the distribution for mean degree ratio of the affected to less-affected sides was computed for the AHT session (Fig. 8b). This is calculated by finding the ratio of the mean degree of connectivity in the post-exposure affected to less-affected limbs, for each of the 32 subjects.

Data availability

All of the data supporting the results in this study are available within the paper and its Supplementary Information. The raw, de-identified patient data are available from the corresponding authors upon reasonable request and subject to Institutional Review Board approval.

Code availability

The programming code for results presented in this manuscript is available from the corresponding authors upon reasonable request.

Received: 30 March 2022; Accepted: 11 July 2022

Published online: 29 July 2022

References

- Kwakkel, G., Kollen, B. J., van der Grond, J. & Prevo, A. J. H. Probability of regaining dexterity in the flaccid upper limb: Impact of severity of paresis and time since onset in acute stroke. *Stroke* **34**, 2181–2186 (2003).
- Chae, J., Yang, G., Park, B. K. & Labatia, I. Delay in initiation and termination of muscle contraction, motor impairment, and physical disability in upper limb hemiparesis. *Muscle Nerve* **25**, 568–575 (2002).
- Sullivan, J. E. & Hedman, L. D. Sensory dysfunction following stroke: Incidence, significance, examination, and intervention. *Top. Stroke Rehabil.* **15**, 200–217 (2008).
- Kang, N., Idica, J., Amitoj, B. & Cauraugh, J. H. Motor recovery patterns in arm muscles: Coupled bilateral training and neuromuscular stimulation. *J. Neuroeng. Rehabil.* **11**, 1–9 (2014).
- Srivatsan, S. et al. Power spectral analysis of surface EMG in stroke: A preliminary study. In *2013 6th International IEEE/EMBS Conference on Neural Engineering (NER)*, 1606–1609 (2013).
- Duncan, P. W. Stroke disability. *Phys. Ther.* **74**, 399–407 (1994).
- Laible, M. et al. Association of activity changes in the primary sensory cortex with successful motor rehabilitation of the hand following stroke. *Neurorehabil. Neural Repair* **26**, 881–888 (2012).
- Mutha, P. K., Stapp, L. H., Sainburg, R. L. & Haaland, K. Y. Frontal and parietal cortex contributions to action modification. *Cortex* **57**, 38–50 (2014).
- Schaefer, S. Y., Haaland, K. Y. & Sainburg, R. L. Hemispheric specialization and functional impact of ipsilesional deficits in movement coordination and accuracy. *Neuropsychologia* **47**, 2953–2966 (2009).

10. Sarlegna, F. R. & Sainburg, R. L. The roles of vision and proprioception in the planning of reaching movements. *Adv. Exp. Med. Biol.* **629**, 317–335 (2009).
11. Bolognini, N., Russo, C. & Edwards, D. J. The sensory side of post-stroke motor rehabilitation. *Restorative Neurol. Neurosci.* **34**, 571–586 (2016).
12. Raghavan, P., Krakauer, J. W. & Gordon, A. M. Impaired anticipatory control of fingertip forces in patients with a pure motor or sensorimotor lacunar syndrome. *Brain* **129**, 1415–1425 (2006).
13. O'Dell, M. W., Lin, C.-C.D. & Harrison, V. Stroke rehabilitation: Strategies to enhance motor recovery. *Ann. Rev. Med.* **60**, 55–68 (2009).
14. Gowland, C. *et al.* Measuring physical impairment and disability with the Chedoke-McMaster stroke assessment. *Stroke* **24**, 58–63 (1993).
15. Gladstone, D. J., Danells, C. J. & Black, S. E. The Fugl-Meyer assessment of motor recovery after stroke: A critical review of its measurement properties. *Neurorehabil. Neural Repair* **16**, 232–240 (2002).
16. Alibiglou, L. & Brown, D. A. Impaired muscle phasing systematically adapts to varied relative angular relationships during locomotion in people poststroke. *J. Neurophysiol.* **105**, 1660–1670 (2011).
17. Wang, L. *et al.* A new EMG-based index towards the assessment of elbow spasticity for post-stroke patients. In *2017 39th Annual International Conference of the IEEE Engineering in Medicine and Biology Society (EMBC)*, 3640–3643 (2017).
18. Angelova, S., Ribagin, S., Raikova, R. & Veneva, I. Power frequency spectrum analysis of surface EMG signals of upper limb muscles during elbow flexion—A comparison between healthy subjects and stroke survivors. *J. Electromyogr. Kinesiol.* **38**, 7–16 (2018).
19. Li, X. *et al.* Power spectral analysis of surface electromyography (EMG) at matched contraction levels of the first dorsal interosseous muscle in stroke survivors. *Clin. Neurophysiol.* **125**, 988–994 (2014).
20. Safavynia, S. A., Torres-Oviedo, G. & Ting, L. H. Muscle synergies: Implications for clinical evaluation and rehabilitation of movement. *Top. Spinal Cord Inj. Rehabil.* **17**, 16–24 (2011).
21. Allen, J. L., Kesar, T. M. & Ting, L. H. Motor module generalization across balance and walking is impaired after stroke. *J. Neurophysiol.* **122**, 277–289 (2019).
22. Sawers, A., Allen, J. L. & Ting, L. H. Long-term training modifies the modular structure and organization of walking balance control. *J. Neurophysiol.* **114**, 3359–3373 (2015).
23. Cheung, V. C. K. *et al.* Stability of muscle synergies for voluntary actions after cortical stroke in humans. *Proc. Natl. Acad. Sci. USA* **106**, 19563–19568 (2009).
24. Laine, C. M. & Valero-Cuevas, F. J. Intermuscular coherence reflects functional coordination. *J. Neurophysiol.* **118**, 1775–1783 (2017).
25. Boonstra, T. W. The potential of corticomuscular and intermuscular coherence for research on human motor control. *Front. Hum. Neurosci.* **7**, 855 (2013).
26. Kerkman, J. N., Daffertshofer, A., Gollo, L. L., Breakspear, M. & Boonstra, T. W. Network structure of the human musculoskeletal system shapes neural interactions on multiple time scales. *Sci. Adv.* **4**, eaat0497 (2018).
27. Walker, S. *et al.* Aging and strength training influence knee extensor intermuscular coherence during low- and High-Force isometric contractions. *Front. Physiol.* **9**, 1933 (2018).
28. Fisher, K. M., Zaaimi, B., Williams, T. L., Baker, S. N. & Baker, M. R. Beta-band intermuscular coherence: A novel biomarker of upper motor neuron dysfunction in motor neuron disease. *Brain* **135**, 2849–2864 (2012).
29. Boonstra, T. W. *et al.* Muscle networks: Connectivity analysis of EMG activity during postural control. *Sci. Rep.* **5**, 17830 (2015).
30. O'Keefe, R. *et al.* Perilaryngeal-Cranial functional muscle network differentiates vocal tasks: A multi-channel sEMG approach. *IEEE Trans. Biomed. Eng.* 1–1 (2022).
31. Imperatori, L. S. *et al.* EEG functional connectivity metrics wPLI and wSMI account for distinct types of brain functional interactions. *Sci. Rep.* **9**, 8894 (2019).
32. Imperatori, L. S. *et al.* Cross-participant prediction of vigilance stages through the combined use of wPLI and wSMI EEG functional connectivity metrics. *Sleep* **44**, zsaa247 (2021).
33. Alonso, J. F. *et al.* MEG connectivity analysis in patients with Alzheimer's disease using cross mutual information and spectral coherence. *Ann. Biomed. Eng.* **39**, 524–536 (2011).
34. Alonso, J. F., Mañanas, M. A., Romero, S., Rojas-Martínez, M. & Riba, J. Cross-conditional entropy and coherence analysis of pharmac-EEG changes induced by alprazolam. *Psychopharmacology* **221**, 397–406 (2012).
35. Wang, Z. J., Lee, P.W.-H. & McKeown, M. J. A novel segmentation, mutual information network framework for EEG analysis of motor tasks. *Biomed. Eng. Online* **8**, 9 (2009).
36. Yin, Z. *et al.* Functional brain network analysis of schizophrenic patients with positive and negative syndrome based on mutual information of EEG time series. *Biomed. Signal Process. Control* **31**, 331–338 (2017).
37. Lu, Y., Bilaloglu, S., Aluru, V. & Raghavan, P. Quantifying feedforward control: A linear scaling model for fingertip forces and object weight. *J. Neurophysiol.* **114**, 411–418 (2015).
38. Bilaloglu, S. *et al.* Effect of blocking tactile information from the fingertips on adaptation and execution of grip forces to friction at the grasping surface. *J. Neurophysiol.* **115**, 1122–1131 (2016).
39. Holobar, A. & Farina, D. Noninvasive neural interfacing with wearable muscle sensors: Combining convolutive blind source separation methods and deep learning techniques for neural decoding. *IEEE Signal Process. Mag.* **38**, 103–118 (2021).
40. Guertin, P. Central pattern generator for locomotion: Anatomical, physiological, and pathophysiological considerations. *Front. Neurol.* **3**, 183 (2013).
41. Huang, H. J. & Ferris, D. P. Computer simulations of neural mechanisms explaining upper and lower limb excitatory neural coupling. *J. Neuroeng. Rehabil.* **7**, 59 (2010).
42. Zehr, E. P. & Duysens, J. Regulation of arm and leg movement during human locomotion. *Neuroscientist* **10**, 347–361 (2004).
43. Chéron, G. *et al.* From spinal central pattern generators to cortical network: Integrated BCI for walking rehabilitation. *Neural Plast.* **2012** (2012).
44. Ting, L. H. & Chvatal, S. A. Decomposing muscle activity in motor tasks, methods and interpretation. In *Motor Control*, 102–138 (Oxford University Press, 2011).
45. McKay, J. L. & Ting, L. H. Functional muscle synergies constrain force production during postural tasks. *J. Biomech.* **41**, 299–306 (2008).
46. Allen, J. L., McKay, J. L., Sawers, A., Hackney, M. E. & Ting, L. H. Increased neuromuscular consistency in gait and balance after partnered, dance-based rehabilitation in Parkinson's disease. *J. Neurophysiol.* **118**, 363–373 (2017).
47. Roh, J., Rymer, W. Z., Perreault, E. J., Yoo, S. B. & Beer, R. F. Alterations in upper limb muscle synergy structure in chronic stroke survivors. *J. Neurophysiol.* **109**, 768–781 (2013).
48. Irastorza-Landa, N. *et al.* Functional synergy recruitment index as a reliable biomarker of motor function and recovery in chronic stroke patients. *J. Neural Eng.* **18**, 046061 (2021).
49. Stinear, C. M. *et al.* PREP2: A biomarker-based algorithm for predicting upper limb function after stroke. *Ann. Clin. Transl. Neurol.* **4**, 811–820 (2017).
50. Milot, M.-H. & Cramer, S. C. Biomarkers of recovery after stroke. *Curr. Opin. Neurol.* **21**, 654–659 (2008).
51. Freedman, D. & Diaconis, P. On the histogram as a density estimator: L 2 theory. *Z. Wahrscheinlichkeitstheorie verw Gebiete* **57**, 453–476 (1981).

52. Sun, C. *et al.* Mutual Information-Based brain network analysis in post-stroke patients with different levels of depression. *Front. Hum. Neurosci.* **12**, 285 (2018).
53. Smith, R. A mutual information approach to calculating nonlinearity. *Stat* **4**, 291–303 (2015).
54. Zhao, J., Zhou, Y., Zhang, X. & Chen, L. Part mutual information for quantifying direct associations in networks. *Proc. Natl. Acad. Sci. USA* **113**, 5130–5135 (2016).
55. Dionisio, A., Menezes, R. & Mendes, D. A. Mutual information: A measure of dependency for nonlinear time series. *Phys. A Stat. Mech. Appl.* **344**, 326–329 (2004).
56. Saramäki, J., Kivelä, M., Onnela, J.-P., Kaski, K. & Kertész, J. Generalizations of the clustering coefficient to weighted complex networks. *Phys. Rev. E Stat. Nonlin. Soft Matter Phys.* **75**, 027105 (2007).
57. Broumi, S., Bakal, A., Talea, M., Smarandache, F. & Vladareanu, L. Applying dijkstra algorithm for solving neutrosophic shortest path problem. In *2016 International conference on advanced mechatronic systems (ICAMechS)*, 412–416 (IEEE, 2016).

Disclaimer

This article reflects the views of the authors and should not be construed to represent FDA's views or policies. The mention of commercial products, their sources, or their use in connection with material reported herein is not to be construed as either an actual or implied endorsement of such products by the Department of Health and Human Services.

Author contributions

S.F.A., R.B., and P.R. conceived the analysis. S.B. and P.R. collected the datasets. S.F.A., R.O.K., and S.J. analyzed the data. S.F.A., R.O.K., and S.Y.S. performed the statistical analysis, interpreted the results, and drafted the manuscript. S.F.A., R.O.K., S.Y.S., and P.R. contributed in revising the manuscript.

Funding

This work was partly supported by the National Science Foundation Grant 2037878 to SFA. Data used in this work was collected with support from the National Institutes of Health Grant 1R01HD071978 to PR.

Competing interests

PR is an inventor on an issued patent for the Sensorimotor Rehabilitator, which was not used in the collection of the data presented in this paper. PR was also not involved in selection of the analysis methods and statistics. The other authors declare no conflicts of interest.

Additional information

Correspondence and requests for materials should be addressed to P.R. or S.F.A.

Reprints and permissions information is available at www.nature.com/reprints.

Publisher's note Springer Nature remains neutral with regard to jurisdictional claims in published maps and institutional affiliations.



Open Access This article is licensed under a Creative Commons Attribution 4.0 International License, which permits use, sharing, adaptation, distribution and reproduction in any medium or format, as long as you give appropriate credit to the original author(s) and the source, provide a link to the Creative Commons licence, and indicate if changes were made. The images or other third party material in this article are included in the article's Creative Commons licence, unless indicated otherwise in a credit line to the material. If material is not included in the article's Creative Commons licence and your intended use is not permitted by statutory regulation or exceeds the permitted use, you will need to obtain permission directly from the copyright holder. To view a copy of this licence, visit <http://creativecommons.org/licenses/by/4.0/>.

© The Author(s) 2022